HHS Public Access

Author manuscript

Opt Lasers Eng. Author manuscript; available in PMC 2017 February 01.

Published in final edited form as:

Opt Lasers Eng. 2016 February ; 77: 92–99. doi:10.1016/j.optlaseng.2015.07.013.

A comparison of 2D and 3D digital image correlation for a membrane under inflation

Barbara J. Murienne[*] and **Thao D. Nguyen**

Department of Mechanical Engineering, Johns Hopkins University, Baltimore, MD, USA

Abstract

Three-dimensional (3D) digital image correlation (DIC) is becoming widely used to characterize the behavior of structures undergoing 3D deformations. However, the use of 3D-DIC can be challenging under certain conditions, such as high magnification, and therefore small depth of field, or a highly controlled environment with limited access for two-angled cameras. The purpose of this study is to compare 2D-DIC and 3D-DIC for the same inflation experiment and evaluate whether 2D-DIC can be used when conditions discourage the use of a stereo-vision system. A latex membrane was inflated vertically to 5.41 kPa (reference pressure), then to 7.87 kPa (deformed pressure). A two-camera stereo-vision system acquired top-down images of the membrane, while a single camera system simultaneously recorded images of the membrane in profile. 2D-DIC and 3D-DIC were used to calculate horizontal (in the membrane plane) and vertical (out of the membrane plane) displacements, and meridional strain. Under static conditions, the baseline uncertainty in horizontal displacement and strain were smaller for 3D-DIC than 2D-DIC. However, the opposite was observed for the vertical displacement, for which 2D-DIC had a smaller baseline uncertainty. The baseline absolute error in vertical displacement and strain were similar for both DIC methods, but it was larger for 2D-DIC than 3D-DIC for the horizontal displacement. Under inflation, the variability in the measurements were larger than under static conditions for both DIC methods. 2D-DIC showed a smaller variability in displacements than 3D-DIC, especially for the vertical displacement, but a similar strain uncertainty. The absolute difference in the average displacements and strain between 3D-DIC and 2D-DIC were in the range of the 3D-DIC variability. Those findings suggest that 2D-DIC might be used as an alternative to 3D-DIC to study the inflation response of materials under certain conditions.

Keywords

Digital image correlation; 3D full-field measurements; 2D profile measurements; Mechanical testing; Inflation

[*]Corresponding author at: The Johns Hopkins University, Department of Mechanical Engineering, Latrobe Hall 200, 3400 N. Charles St., Baltimore, MD 21218, USA. Tel.: +1 410 516 8781; fax: +1 410 516 7254. bmurien1@jhu.edu (B.J. Murienne).

Conflict of interest

None declared.

1. Introduction

Digital image correlation (DIC) is a non-contact method used to calculate the 2D or 3D full-field surface displacement response of structures to mechanical loading. From the displacement field, the surface strain field can be calculated to characterize the local mechanical behavior of the specimens. DIC has been utilized to characterize the mechanical properties of a wide range of materials, including biological materials [1–10].

The two-dimensional version of DIC (2D-DIC) is applied to a series of images of a deforming planar specimen acquired by a single camera. The surface of the specimen is speckled to present a random intensity pattern. Reference subsets in the reference image (typically the first image) are compared to subsets in a deformed image (any subsequent image) to find the target subset, which is the subset in the deformed image that shows the maximum pattern similarity with the reference subset. The location of the target subset is usually found based on a cross-correlation criterion or minimum sum-squared difference correlation criterion [11]. Zero-order or first-order shape functions are commonly used to describe the reference subset displacement/ deformation in the deformed image during the matching process [11]. Since first-order shape functions are more accurate but also more computationally expensive, most commercially available software use zero-order shape functions. Since there is no one-to-one pixel correspondence between the reference and deformed subsets, sub-pixel intensities in the deformed image are obtained using common interpolation schemes, such as bicubic interpolation, prior to matching [11]. Alternatively, sub-pixel interpolation of the correlation coefficient can be performed [12,13]. This process returns the new 2D positions of points on the specimen surface, from which 2D displacement vectors are calculated. This process can be repeated for all deformed images to obtain the 2D displacement of the specimen surface throughout the deformation. The main source of error in 2D-DIC is the image correlation error, which is the error in the pattern matching process between different image frames. It is a function of the camera noise, image distortion, illumination conditions, speckle pattern, how parallel the camera sensor and specimen are and matching process (subset size, shape function, sub-pixel interpolation scheme, correlation criterion) [11].

In comparison, the three-dimensional version of DIC (3D-DIC) operates on a series of image pairs of a deforming object acquired by a two-camera stereo-vision system. The images from the reference pair are correlated to match image subsets between cameras, and the 3D surface geometry is reconstructed using the camera intrinsic and extrinsic parameters, and triangulation. The intrinsic parameters describe the characteristics of each camera-lens system, such as the location of the intersection between the optical axis and the sensor plane, the skew of the sensor plane, the focal length and the distortion coefficient. The extrinsic parameters describe the relative position of the camera-lens systems, including their distance and orientation [14]. The changes in 3D surface geometry throughout the deformation are then obtained through the correlation of each deformed image pair with the reference pair, and triangulation. This process returns the new 3D positions of points on the specimen surface from which 3D displacement vectors are calculated. 3D-DIC is associated with two main sources of error: a correlation error and a 3D reconstruction error [15,16]. The reconstruction error is the error in the imaging system calibration. It is mainly a

function of the camera positioning (stereo-angle) and calibration, and the objective focal length [15,16].

The use of 2D-DIC is often limited by the 3D nature of the material structure and deformation, and by its high sensitivity to out-of-plane motions, which generate significant errors in in-plane displacement and strain measurements [17,18]. Therefore, 2D-DIC is optimal for deformation tracking of planar specimens showing a small out-of-plane contraction under planar deformation, whereas 3D-DIC is recommended for non-planar specimens or planar specimens undergoing significant rotations and out-of-plane displacements. However, some experimental conditions discourage the use of 3D-DIC, such as (1) high magnification, and therefore small depth of field [19], which can be an issue if the specimen deforms substantially in the out-of-plane direction, (2) a highly controlled environment during mechanical testing, which might limit the accessibility for two-angled cameras [20], (3) high-speed experiments, for which both cameras need to be perfectly synchronized [21], or (4) stiff membranes, for which the out-of-plane deformation is small and might not be accurately measured by 3D-DIC. Some of these conditions have motivated recent developments of techniques to measure 3D deformations using images acquired with a single camera [20–24]. Stereo-microscopy is also becoming increasingly popular for measurements on the microscale [25–27] however, it still suffers from a small depth of field at high magnification, a lower sensitivity in the out-of-plane measures compared to the in-plane measures [27] and a higher cost than traditional stereo-vision systems.

In this study, we aimed to compare the displacements and strain obtained from 2D-DIC and 3D-DIC for the same inflation test. Inflation testing is widely used to characterize the mechanical behavior of biological materials [4–6,8,10,19,28], as well as non-biological tubular materials [29] and thin films [30–34]. We developed an experimental setup to measure the deformation of a bulged membrane in response to pressure increase. The pressurization of the initially bulged membrane imposes a uniform strain condition away from the clamps.

2. Methods

This section describes the methods used to obtain the horizontal and vertical displacement components and meridional strain from 2D-DIC and 3D-DIC.

2.1. Specimen preparation

A 0.2032±0.0508 mm thick latex membrane (Abrasion-resistant natural latex rubber film, 85995K13, McMaster-Carr, Princeton, NJ) was glued flat to a custom-made acrylic holder with a 20.5 mm circular opening. The specimen was transilluminated using a lamp with a diameter much larger than that of the holder to ensure a uniform illumination of the membrane. Images of the transilluminated specimen showed variations in light intensity across the membrane, which corresponded to thickness variations and a distinct material texture (Fig. 1). The membrane was speckled with black India ink (Fig. 2(c) and (d)) using an airbrush (ECL4500 HP-CS, Iwata Medea, Portland, OR) to allow for DIC deformation tracking.

2.2. Inflation testing

The inflation test method used in this study was previously described [10]. Briefly, the latex specimen was secured onto a custom inflation chamber through the holder. The pressure was increased by the controlled injection of water into the chamber using a MTS-driven syringe pump (MTS, Eden Prairie, MN). The pressure in the chamber was measured using a high precision pressure transducer (TJE, Honeywell, Columbus, OH). The membrane was first equilibrated at the baseline pressure 0.28 kPa for 30 min and then subjected to a pressure-controlled load test from the baseline pressure to 7.87 kPa at 0.13 kPa/s.

2.3. Imaging

The deforming membrane was imaged simultaneously by a stereo-vision system mounted above the specimen and a mono-vision system positioned to the side of the inflation chamber (Fig. 2 (a) and (b)). The stereo-vision system consisted of two 2 Mpixels monochrome cameras (GRAS-20S4M-C, Point Grey, Richmond, BC, Canada) fitted with 35 mm focal length objectives (Xenoplan 1.9/35 mm-0901, Schneider Optics, Hauppauge, NY), and oriented with a 24° stereo angle (Fig. 2(a)) that acquired top-down images of the membrane. A third camera with the same characteristics was positioned to capture images of the membrane in profile with the same 0.025 mm/pixel image resolution as the stereo-vision system (Fig. 2(b)). The three cameras were synchronized to simultaneously image the membrane using Vic-Snap 2009 (Correlated Solutions Inc., Columbia, SC). The static error and uncertainty in the 2D-DIC and 3D-DIC displacement components and meridional strain were calculated from the correlation of three sequential images taken at a near zero pressure, 0.28 kPa and after the specimen was left to equilibrate for 30 min, to minimize the effect of creep. The static error was defined as the mean of the static displacements and meridional strain measured, while the static uncertainty was defined as the standard deviation of the measurements from the mean. We used a finite pressure to measure the static error and uncertainty rather than a zero pressure to ensure the membrane was unwrinkled. We used a high reference pressure, 5.41 kPa, for the inflation test to start from a bulged, spherical cap, configuration. This allowed a central region of uniform strain to develop from inflation to the higher 7.87 kPa pressure. During inflation from baseline to 7.87 kPa, images were acquired every 2 s.

2.4. Data analysis

2.4.1. 3D data analysis—The 3D-DIC analysis was performed on the image pairs obtained from the stereo-vision system using Vic-3D 2009 (Correlated Solutions, Columbia, SC). We used a 45-pixel correlation window size and a 5-pixel step size, which provided reference position and displacement vectors on a 2D Cartesian grid with a 0.125 mm spacing. We assumed that away from the boundaries, the reference bulged configuration can be described as a sphere, and fit an equation for a generalized sphere to the position vectors. The fit returned a radius R_{3D} = 15:7 mm for the spherical cap with a negligible average residual of 9.54e-5 mm. Using R_{3D}, we created a spherical grid, spanning 360° in the circumferential θ direction with a 3° spacing and 14° in the meridional ϕ direction with a 1° spacing, and interpolated the displacement vectors onto the spherical grid using the Matlab function spherefit.m (Levente Hunyadi, 2010). The transformation thus provided reference

positions (X, Y, Z) and displacements (U_x, U_y, U_z) at 1° intervals along 120 meridians. The horizontal displacement component U_ξ in the projected radial direction $\xi = R_{3D} \sin(\phi)$ along a meridian with angle θ (Fig. 2(c)) was calculated at each grid point from the interpolated displacements as

$$U_\xi = U_x \cos(\theta) + U_y \sin(\theta). \quad (1)$$

The interpolated U_z provided the vertical displacement component in the vertical direction z. The meridional strain was evaluated from the stretch of the reference spherical grid. At each grid point n along a meridian, the deformed positions were calculated as $x_n = X_n + U_{x_n}$, $y_n = Y_n + U_{y_n}$, $z_n = Z_n + U_{z_n}$. The reference length L_{φ_n} and deformed length l_{φ_n} of the grid were evaluated as

$$L_{\varphi_n} = \sqrt{(X_{n+1} - X_{n-1})^2 + (Y_{n+1} - Y_{n-1})^2 + (Z_{n+1} - Z_{n-1})^2},$$
$$l_{\varphi_n} = \sqrt{(x_{n+1} - x_{n-1})^2 + (y_{n+1} - y_{n-1})^2 + (z_{n+1} - z_{n-1})^2}. \quad (2)$$

The meridional stretch $\lambda_{\phi\phi}$ and Green–Lagrange strain $E_{\phi\phi}$ were evaluated at each grid point using the reference and deformed grid lengths as

$$\lambda_{\varphi\varphi_n} = \frac{l_{\varphi_n}}{L_{\varphi_n}}, \quad E_{\varphi\varphi_n} = \frac{1}{2}(\lambda^2_{\varphi\varphi_n} - 1). \quad (3)$$

2.4.2. 2D data analysis—The 2D-DIC analysis was performed on images obtained from the mono-vision system using Vic-2D 2009 (Correlated Solutions, Columbia, SC). We used the same correlation window size and step size as for the 3D-DIC analysis. The horizontal and vertical displacement components (U_ξ, U_z) were extracted for a series of points on the membrane boundary in the reference configuration, which corresponded to the θ_{2D} and θ_{2D} +180° meridians in Fig. 2 (c). The location (X, Z) of those points coincided with the location of the 3D-DIC reference spherical grid points along the ξ direction from the membrane center. The center of the membrane in profile was calculated by fitting a generalized circle to the position vectors on the membrane boundary using the Matlab function CircleFitByTaubin.m (Nikolai Chrenov, 2009). The meridional strain was calculated from the 2D reference positions (X, Z) and displacements (U_ξ, U_z) using the 2D version of Eqs. (2) and (3).

3. Results

3.1. 3D regional variations

To examine the spatial variations in the inflation response, we divided the specimen into 4 quadrants (Fig. 2(c)) and averaged the 3D-DIC displacements and meridional strains over the 30 meridians of each quadrant, at each ξ position. We also averaged the 3D-DIC displacements and meridional strains at each ξ position over all 120 meridians. The results are plotted as a function of the horizontal position ξ in Fig. 3. Significant variations were observed in the 3D-DIC measurements along ξ across the membrane. The maximum

absolute difference along ξ between quadrants were 0.016 mm between quadrants 2 and 4 for the horizontal displacement, 0.033 mm between quadrants 3 and 4 for the vertical displacement, and 0.033 between quadrants 2 and 4 for the meridional strain. The variation in displacements and strain along ξ were smaller when the results were averaged over the entire membrane. Due to the large regional variations in the 3D-DIC measurements, which could be partly due to the membrane heterogeneity shown in Fig. 1, the 2D-DIC measurements were compared to the 3D-DIC measurements of quadrants 1 and 3 only, which contained the 2D meridians.

3.2. Static noise

The probability distributions of the static noise for 2D-DIC and 3D-DIC displacement components and strain were calculated using a 0.0005 bin size and are plotted in Fig. 4. Fifteen additional values were extracted along each 2D meridians to obtain a representative statistical distribution. The probability for each bin was calculated as the number of measurements in the bin divided by the total number of measurements. The static error was defined as the mean of each distribution and the static uncertainty was defined as the standard deviation from the mean. For the horizontal displacements, the absolute error was 13 times higher for 2D-DIC than for 3D-DIC, whereas the uncertainty in 2D-DIC was only twice the uncertainty in 3D-DIC. For the vertical displacements, the absolute error was 0.7 times smaller for 2D-DIC than for 3D-DIC, and the uncertainty in 2D-DIC was 0.3 times smaller than the uncertainty in 3D-DIC. For the meridional strain, the absolute error was 0.9 times smaller for 2D-DIC than 3D-DIC, whereas the uncertainty in 2D-DIC showed a value 5 times higher than the uncertainty in 3D-DIC.

3.3. Displacements

The 3D-DIC displacement measurements for pressurization from 5.41 kPa to 7.87 kPa are plotted in Fig. 5(a) and (b) along the horizontal direction ξ for the 60 meridians of quadrants 1 and 3. The 2D-DIC displacement measurements for the 2 meridians of the membrane profile are also plotted for comparison. The variation in displacements were generally higher for 3D-DIC than 2D-DIC, for both the horizontal and vertical displacements, though the difference was significantly larger for the vertical displacement. The 3D-DIC vertical displacements were also generally larger than those measured by 2D-DIC. For 3D-DIC, the variation in the vertical displacement was larger than for the horizontal displacement, whereas 2D-DIC showed similar variations for both displacement components. To further compare the variation in 2D-DIC and 3D-DIC measurements, the range in the displacement components was calculated at each ξ position as the difference between the maximum and minimum displacement values among the 60 meridians or 2 meridians considered. Further averaging over all ξ positions gave an average range for the horizontal displacement of 0.0044 mm for 2D-DIC and 0.017 mm for 3D-DIC. The average range for the vertical displacement was 0.0035 mm for 2D-DIC and 0.052 mm for 3D-DIC. The absolute difference between the average 3D-DIC and 2D-DIC displacements was calculated as the absolute value of the difference between the 3D-DIC displacements averaged over the 60 meridians, and the 2D-DIC displacements averaged over the 2 meridians. The results are plotted for the horizontal and vertical displacements along ξ in Fig. 5(c). Further averaging

over all ξ positions gave an average absolute difference of 0.0024 mm for the horizontal displacement and 0.014 mm for the vertical displacement.

3.4. Meridional strain

The meridional strain is plotted as a function of the horizontal position ξ for the 2D meridians and 3D meridians from quadrants 1 and 3 in Fig. 6(a) for comparison between 2D-DIC and 3D-DIC. The variation in 2D-DIC and 3D-DIC strain were comparable over the 4 mm region around the membrane apex. We assumed that the meridional strains were uniform within the central 4 mm region, and plotted the 2D-DIC and 3D-DIC strains as probability distributions using a 0.0020 bin size as shown in Fig. 6(b). The probability distributions for the meridional strain were similar for 2D-DIC and 3D-DIC. The means of the 2D-DIC and 3D-DIC distributions differed by 0.0029, while the standard deviations were nearly identical.

4. Discussion

In this study, we compared 2D-DIC and 3D-DIC outcomes for the inflation of a latex membrane. We first measured the baseline error and uncertainty for the static membrane under a near zero pressure. The baseline absolute error and uncertainty in the horizontal displacement were larger for 2D-DIC than 3D-DIC. This could be due to a higher noise within the correlation window at the membrane boundary, as it was partially on the background and on the speckle pattern, which probably affected the subset correlation and therefore the displacement measurements. In addition, 2D-DIC showed a larger baseline uncertainty in the horizontal displacement than in the vertical displacement. This might be due to the contrast of the membrane boundary imaged in profile being lower, and therefore more susceptible to noise, in the meridional direction (along the membrane) than in the vertical direction, where approximately half of the correlation window contained the black background. The baseline uncertainty in the vertical displacement was larger for 3D-DIC than 2D-DIC. In addition, 3D-DIC showed a larger baseline absolute error and uncertainty for the vertical displacement than for the horizontal displacement, which was consistent with other studies [14,35]. Both findings suggest that noise has a greater effect on the out-of-plane measures compared to the in-plane measures for 3D-DIC, possibly due to a higher sensibility of the 3D reconstruction process to noise. The effect of measuring the displacements at the membrane boundary, where the correlation window partially contains some background may explain why we measured a 2D-DIC displacement uncertainty up to 0.068 pixels, which was 10 times higher than the maximum 0.006 pixels position uncertainty measured by Ke et al. [35] for a static planar object. Similarly for 3D-DIC, the 0.0322 pixels and 0.128 pixels horizontal and vertical displacement uncertainties reported here were about 10 times higher than the maximum 0.0030 pixels and 0.0093 pixels position uncertainties reported by Ke et al. [35] for a planar object. However, Hu et al. [14] numerically and experimentally reported significantly higher positional uncertainties than those reported here, for static cylinders. This suggests that the baseline positional uncertainty of 3D-DIC due to noise is higher for curved objects than planar objects. The baseline uncertainty in the meridional strain was higher for 2D-DIC than 3D-DIC. This can be explained by the interpolation of displacements in the 3D-DIC analysis, whereas no

interpolation was performed in the 2D-DIC analysis. We obtained a 4400 microstrain uncertainty from 2D-DIC and a 818 microstrain from 3D-DIC, whereas Ke et al. [35] reported a 3D-DIC in-plane strain uncertainty of 90 microstrain from static tests of a planar object. In addition to using a planar object, the smaller strain uncertainty obtained by Ke et al. [35] can be attributed to the use of a spatial averaging scheme for the strain calculation.

The variation in displacements and meridional strain increased significantly for 2D-DIC and 3D-DIC with inflation. This could be partly attributed to the variations in the material properties and thickness of the membrane shown in Fig. 1. The membrane exhibited a distinct texture, appearing as parallel lines in Fig. 1, that may have originated from the manufacturing process of the rubber sheet. Under inflation, 3D-DIC also showed a larger variation in the vertical (out-of-plane) displacement than in the horizontal (in-plane) displacement, as reported in this study and others under static conditions [14,35]. In contrast, 2D-DIC showed similar variations for both displacement components. The variation in displacements were generally larger for 3D-DIC than 2D-DIC, and the difference was significantly larger for the vertical displacement, suggesting again additional sources of variability in the 3D-DIC out-of-plane measures. Moreover, the absolute difference between the average 3D-DIC and 2D-DIC displacements across the meridians were within the range of 3D-DIC for both displacement components. Interestingly, the uncertainty in the meridional strain was nearly identical for both DIC methods. This could be due to the interpolation of the displacements on a spherical grid for the 3D-DIC data analysis. For 3D-DIC, we interpolated the raw displacement data onto a spherical grid, which introduced a degree of smoothing to the displacement and strain calculations. Interpolation of the data onto a coarser spherical grid resulted in a smoother strain field. A reasonable interpolation grid seemed to be a grid slightly more sparse than the array of data points given by DIC, to guarantee the accurate interpolation of the displacements while preventing over-smoothing and the loss of local information. For this study, an interpolation grid spacing of $\Delta\phi = 1°$ corresponded to a grid size of 0.27 mm in the meridional direction, which was twice the 0.125 mm step size used for the DIC analysis. However, the absolute difference between the mean of the 3D-DIC and 2D-DIC strain distributions was within the range of the 3D-DIC strain uncertainty. The strain uncertainty of 8000 microstrain reported here for both DIC methods was an order of magnitude larger than the 800 microstrain uncertainty reported by Sutton et al. [4] for the translation of a cylinder. Although Sutton et al. [4] used a smoothing scheme to calculate strains, this might suggest that 3D deformation generates higher uncertainties than translation. The variation in displacements and meridional strain did not show an increasing or decreasing trend from the membrane apex towards the holder for the central 8.0 mm apical region for 2D-DIC and 3D-DIC.

In this study we did not use a telecentric lens and did not correct for lens distortions, which naturally introduced some bias in the 2D-DIC measurements. 2D-DIC was probably affected by the change in magnification with depth due to the membrane curvature, especially without the use of a telecentric lens for the image acquisition [36]. However, the 2D-DIC displacements were extracted at the membrane boundary to limit the effect of curvature and the focus of the 2D-DIC camera system was set to the membrane boundary at the baseline pressure to minimize the effect of defocus with inflation. The maximum out of the (ξ-z)

plane dimension of the bulged membrane at maximum pressure that was included in the correlation window was calculated to be 4 mm, which was within the depth of field of the 2D-DIC system. Thus, the effect of defocusing on the 2D-DIC measurements at the membrane boundary could be considered small. 2D-DIC was also probably affected by lens distortions [37,38]. The main lens distortions include radial and tangential distortions [38], although tangential distortion effects can usually be ignored [39]. However, the portion of the membrane considered in this study was far away from the image edges where the radial distortion is greater. Moreover, no increase or decrease in the 2D-DIC variations or difference with the 3D-DIC measurements was observed along the meridians, which favors a small effect of lens distortion compared to other effects.

The results suggest that 3D-DIC should be used to fully characterize the mechanical behavior of heterogeneous materials and investigate the anisotropy of their response to inflation. However, 2D-DIC might be used as an alternative to 3D-DIC under certain conditions, such as an inflation, where the deformation can be imaged in profile in the plane of the 2D-DIC camera system. Since 3D-DIC has a larger error and uncertainty in the vertical displacement than in the horizontal displacement, 2D-DIC may provide a comparatively accurate alternative method to measure the deformation of stiff membranes, for which the vertical displacements are comparable to the errors of the 3D-DIC system, and of small specimens, where large deformations would exceed the small depth of field of a high magnification 3D-DIC camera system. In addition, 2D-DIC can be used to overcome the camera synchronization issue in high-speed experiments and space limitation for two-angled cameras in highly controlled experimental environments.

5. Conclusion

In conclusion, we compared 2D-DIC and 3D-DIC outcomes for a simple 3D deformation state, a membrane under inflation. We found that the baseline uncertainty in the horizontal displacement and meridional strain were smaller for 3D-DIC than 2D-DIC, but the opposite was observed for the vertical displacement, for which 2D-DIC showed a smaller baseline uncertainty. The baseline absolute error was similar for both DIC methods for the vertical displacement and strain, but it was larger for 2D-DIC than 3D-DIC for the horizontal displacement. Inflation generally produced higher variations than static conditions for both methods. Under inflation, the variability in both displacement components were larger for 3D-DIC than 2D-DIC, but the uncertainty in the meridional strain was similar for both DIC methods. The absolute difference between the average displacement and strain data from 2D-DIC and 3D-DIC were in the range of the 3D-DIC variability. The results suggest that 2D-DIC might be used as an alternative to 3D-DIC to study the inflation response of specimens under certain conditions.

Acknowledgments

This work was supported by the NIH, grant number EY021500 (PI: Nguyen), and by the US Army Medical Research, Vision Research Program under grant number W81XWH-10-1-0766.

Biographies

Barbara J. Murienne received a M.Sc. in Bioengineering from the Swiss Federal Institute of Technology in Lausanne (EPFL) in 2009. After working as a research associate at Imperial College London, she joined Professor Nguyen's group at Johns Hopkins University in 2011. She currently pursues a Ph.D. in Mechanical Engineering focusing on ocular biomechanics.

Thao D. Nguyen is an Associate Professor in the departments of Mechanical Engineering and Materials Science at The Johns Hopkins University. Dr. Nguyen obtained her S.B. in Mechanical Engineering from MIT, in 1998, and M.S. and Ph.D. in Mechanical Engineering from Stanford, in 2004. She worked as a research scientist at Sandia National Laboratories in Livermore, CA, before joining Johns Hopkins, in 2007. Her research focuses on experimental and computational biomechanics of soft tissues and mechanics of stimuli-responsive polymers.

References

1. Wang CC, Deng JM, Ateshian GA, Hung CT. An automated approach for direct measurement of two-dimensional strain distributions within articular cartilage under unconfined compression. J Biomech Eng. 2002; 124(5):557–67. [PubMed: 12405599]
2. Zhang D, Eggleton CD, Arola DD. Evaluating the mechanical behavior of arterial tissue using digital image correlation. Exp Mech. 2002; 42(4):409–16.
3. Zhang D, Arola DD. Applications of digital image correlation to biological tissues. J Biomed Opt. 2004; 9(4):691–9. [PubMed: 15250755]
4. Sutton M, Ke X, Lessner S, Goldbach M, Yost M, Zhao F, et al. Strain field measurements on mouse carotid arteries using microscopic three-dimensional digital image correlation. J Biomed Mater Res Part A. 2008; 84(1):178–90.
5. Myers KM, Coudrillier B, Boyce BL, Nguyen TD. The inflation response of the posterior bovine sclera. Acta Biomater. 2010; 6(11):4327–35. [PubMed: 20558331]
6. Coudrillier B, Tian J, Alexander S, Myers KM, Quigley HA, Nguyen TD. Biomechanics of the human posterior sclera: age- and glaucoma-related changes measured using inflation testing. Investig Ophthalmol Vis Sci. 2012; 53(4):1714–28. [PubMed: 22395883]

7. Soons J, Lava P, Debruyne D, Dirckx J. Full-field optical deformation measurement in biomechanics: digital speckle pattern interferometry and 3D digital image correlation applied to bird beaks. J Mech Behav Biomed Mater. 2012; 14:186–91. [PubMed: 23026697]
8. Tonge TK, Atlan LS, Voo LM, Nguyen TD. Full-field bulge test for planar anisotropic tissues: part I—experimental methods applied to human skin tissue. Acta Biomater. 2013; 9(4):5913–25. [PubMed: 23261928]
9. Tonge TK, Murienne BJ, Coudrillier B, Alexander S, Rothkopf W, Nguyen TD. Minimal preconditioning effects observed for inflation tests of planar tissues. J Biomech Eng. 2013; 135(11): 114502. [PubMed: 23897279]
10. Murienne BJ, Jefferys JL, Quigley HA, Nguyen TD. The effects of glycosaminoglycan degradation on the mechanical behavior of the posterior porcine sclera. Acta Biomater. 2015; 12:195–206. [PubMed: 25448352]
11. Pan B, Qian K, Xie H, Asundi A. Two-dimensional digital image correlation for in-plane displacement and strain measurement: a review. Meas Sci Technol. 2009; 20(6):062001.
12. Wattrisse B, Chrysochoos A, Muracciole JM, Némoz-Gaillard M. Kinematic manifestations of localisation phenomena in steels by digital image correlation. Eur J Mech-A/Solids. 2001; 20(2): 189–211.
13. Cheng P, Menq CH. Cancelling bias induced by correlation coefficient interpolation for sub-pixel image registration. Meas Sci Technol. 2013; 24(3):035404.
14. Hu Z, Xie H, Lu J, Wang H, Zhu J. Error evaluation technique for three-dimensional digital image correlation. Appl Opt. 2011; 50(33):6239–47. [PubMed: 22108882]
15. Becker T, Splitthof K, Siebert T, Kletting P. Error estimations of 3D digital image correlation measurements. Proceedings of SPIE. 2006; 6341:63410F.
16. Siebert T, Becker T, Spiltthof K, Neumann I, Krupka R. Error estimations in digital image correlation technique. Appl Mech Mater. 2007; 7:265–70.
17. Haddadi H, Belhabib S. Use of rigid-body motion for the investigation and estimation of the measurement errors related to digital image correlation technique. Opt Lasers Eng. 2008; 46(2): 185–96.
18. Sutton M, Yan J, Tiwari V, Schreier H, Orteu J. The effect of out-of-plane motion on 2D and 3D digital image correlation measurements. Opt Lasers Eng. 2008; 46(10):746–57.
19. Myers KM, Cone FE, Quigley HA, Gelman S, Pease ME, Nguyen TD. The in vitro inflation response of mouse sclera. Exp Eye Res. 2010; 91(6):866–75. [PubMed: 20868685]
20. Xia S, Gdoutou A, Ravichandran G. Diffraction assisted image correlation: a novel method for measuring three-dimensional deformation using two-dimensional digital image correlation. Exp Mech. 2013; 53(5):755–65.
21. Pankow M, Justusson B, Waas AM. Three-dimensional digital image correlation technique using single high-speed camera for measuring large out-of-plane displacements at high framing rates. Appl Opt. 2010; 49(17):3418–27. [PubMed: 20539362]
22. Tay CJ, Quan C, Huang Y, Fu Y. Digital image correlation for whole field out-of-plane displacement measurement using a single camera. Opt Commun. 2005; 251(1):23–36.
23. Quan C, Tay CJ, Sun W, He X. Determination of three-dimensional displacement using two-dimensional digital image correlation. Appl Opt. 2008; 47(4):583–93. [PubMed: 18239719]
24. Genovese K, Casaletto L, Rayas J, Flores V, Martinez A. Stereo-Digital Image Correlation (DIC) measurements with a single camera using a biprism. Opt Lasers Eng. 2013; 51(3):278–85.
25. Schreier H, Garcia D, Sutton M. Advances in light microscope stereo vision. Exp Mech. 2004; 44(3):278–88.
26. Zhang D, Luo M, Arola DD. Displacement/strain measurements using an optical microscope and digital image correlation. Opt Eng. 2006; 45(3):033605.
27. Hu Z, Luo H, Du Y, Lu H. Fluorescent stereo microscopy for 3D surface profilometry and deformation mapping. Opt Express. 2013; 21(10):11808–18. [PubMed: 23736402]
28. Girard MJ, Suh JKF, Bottlang M, Burgoyne CF, Downs JC. Scleral biomechanics in the aging monkey eye. Investig Ophthalmol Vis Sci. 2009; 50(11):5226–37. [PubMed: 19494203]

29. Sokolowski T, Gerke K, Ahmetoglu M, Altan T. Evaluation of tube formability and material characteristics: hydraulic bulge testing of tubes. J Mater Process Technol. 2000; 98(1):34–40.
30. Vlassak J, Nix W. A new bulge test technique for the determination of Young's modulus and Poisson's ratio of thin films. J Mater Res. 1992; 7(12):3242–9.
31. Karimi A, Shojaei O, Kruml T, Martin J. Characterisation of TiN thin films using the bulge test and the nanoindentation technique. Thin Solid Films. 1997; 308:334–9.
32. Xiang, Y.; Chen, X.; Vlassak, JJ. MRS Proceedings. Vol. 695. Cambridge Univ Press; 2001. The mechanical properties of electroplated Cu thin films measured by means of the bulge test technique; p. L4-9.
33. Huang C, Lou W, Tsai C, Wu TC, Lin HY. Mechanical properties of polymer thin film measured by the bulge test. Thin Solid Films. 2007; 515(18):7222–6.
34. Berdova M, Ylitalo T, Kassamakov I, Heino J, Törmä PT, Kilpi L, et al. Mechanical assessment of suspended ALD thin films by bulge and shaft-loading techniques. Acta Mater. 2014; 66:370–7.
35. Ke XD, Schreier H, Sutton M, Wang Y. Error assessment in stereo-based deformation measurements. Exp Mech. 2011; 51(4):423–41.
36. Pan B, Yu L, Wu D. High-accuracy 2D digital image correlation measurements with bilateral telecentric lenses: error analysis and experimental verification. Exp Mech. 2013; 53(9):1719–33.
37. Tang ZZ, Liang J, Guo C, Wang YX. Photogrammetry-based two-dimensional digital image correlation with nonperpendicular camera alignment. Opt Eng. 2012; 51(2):023602–11.
38. Lava P, van Paepegem W, Coppieters S, De Baere I, Wang Y, Debruyne D. Impact of lens distortions on strain measurements obtained with 2D digital image correlation. Opt Lasers Eng. 2013; 51(5):576–84.
39. Tsai RY. A versatile camera calibration technique for high-accuracy 3D machine vision metrology using off-the-shelf TV cameras and lenses. IEEE J Robot Autom. 1987; 3(4):323–44.

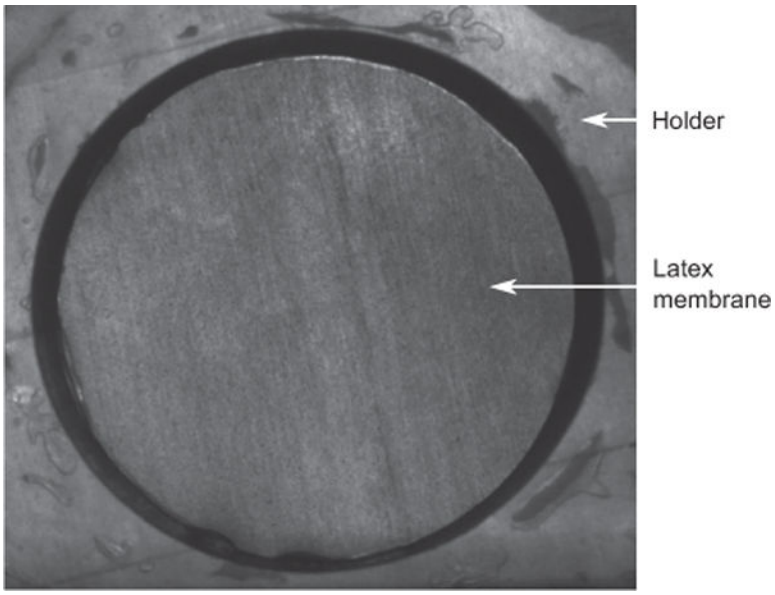

Fig. 1.
Transilluminated latex membrane showing variations in light intensity.

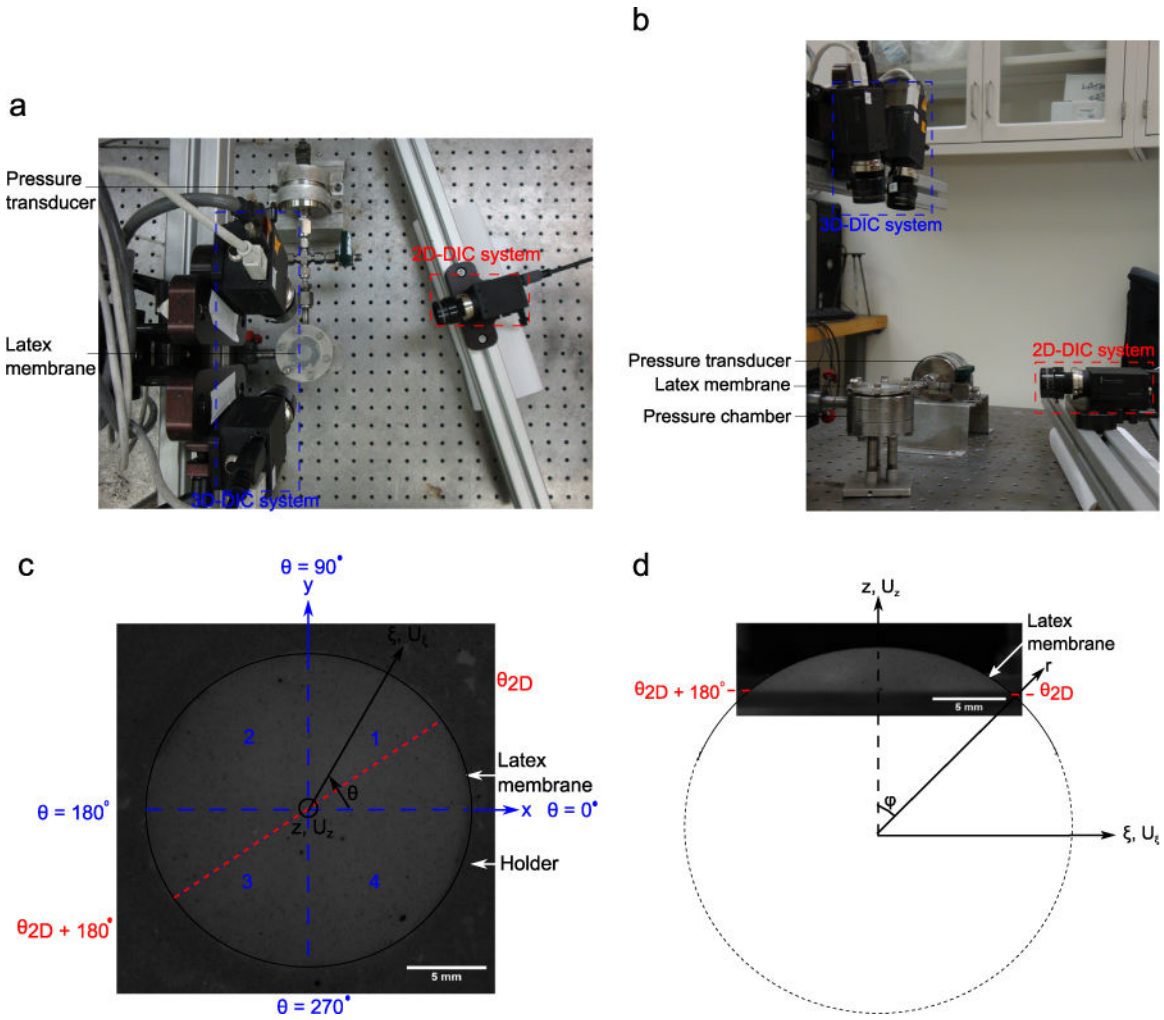

Fig. 2.

(a) Top view and (b) side view of the inflation experimental setup, showing the latex membrane, inflation chamber, pressure transducer, stereo-vision system (blue) and mono-vision system (red). (c) Top view and (d) side view of the inflated latex membrane. The blue axes define the 4 quadrants used to analyze the 3D-DIC data and the red axis defines the direction of the profile-edge imaged by the mono-vision system.

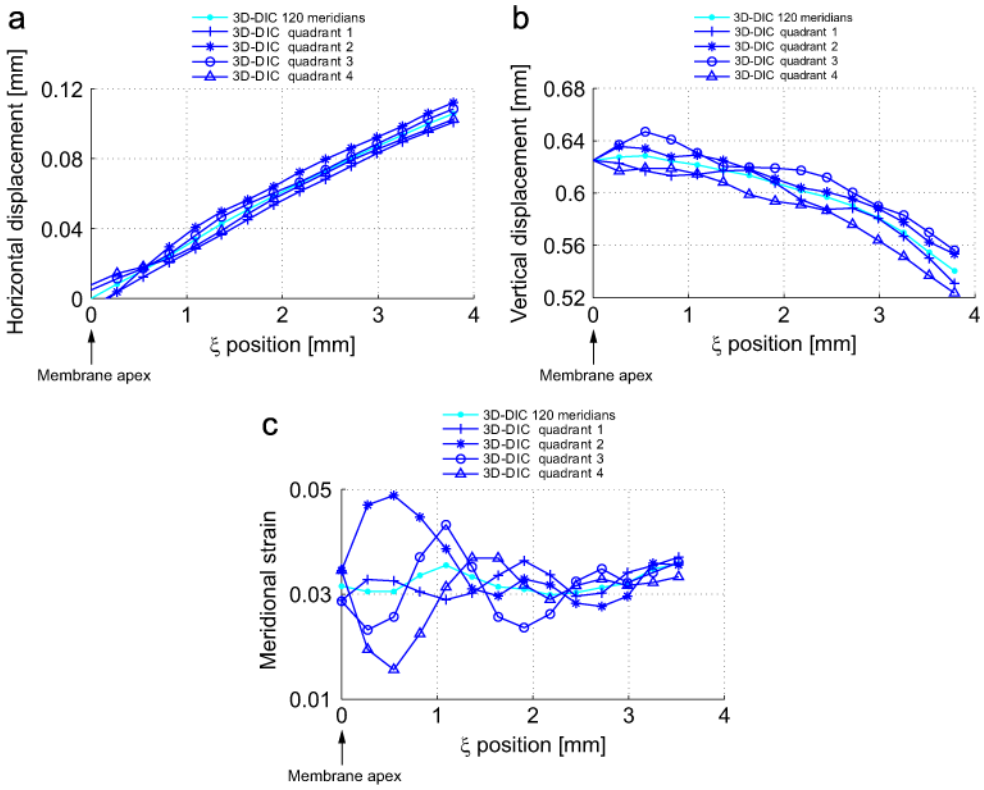

Fig. 3.

3D-DIC (a) horizontal displacement, (b) vertical displacement and (c) meridional strain averaged over each quadrant of the membrane and over the entire membrane, at each ξ position.

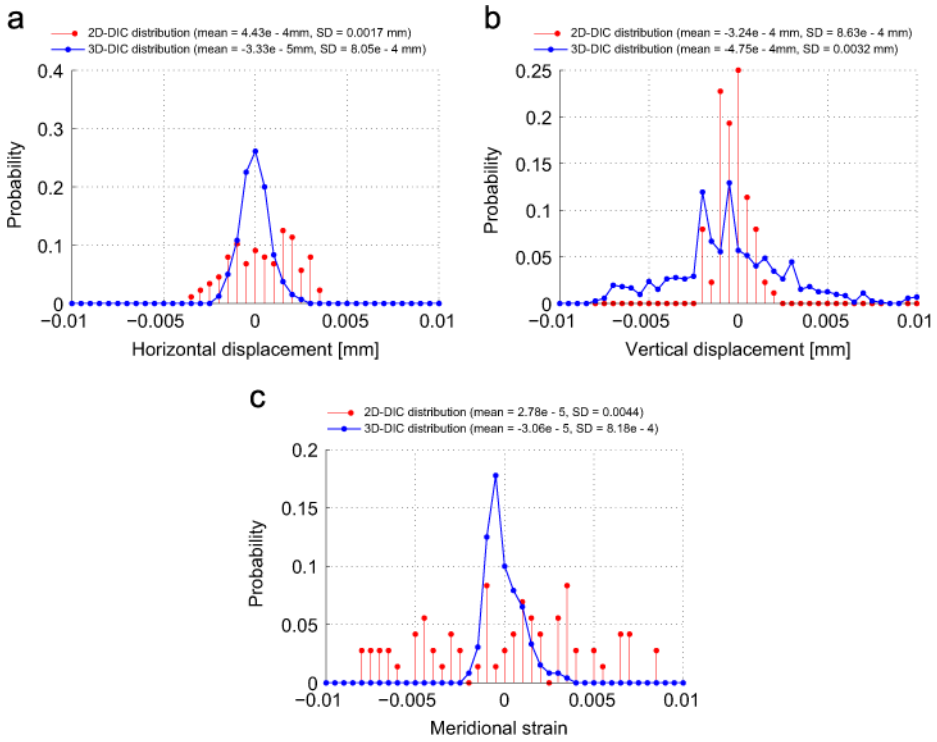

Fig. 4.

Probability distributions for the static noise for 2D-DIC and 3D-DIC (a) horizontal displacement, (b) vertical displacement and (c) meridional strain, using a 0.0005 bin size.

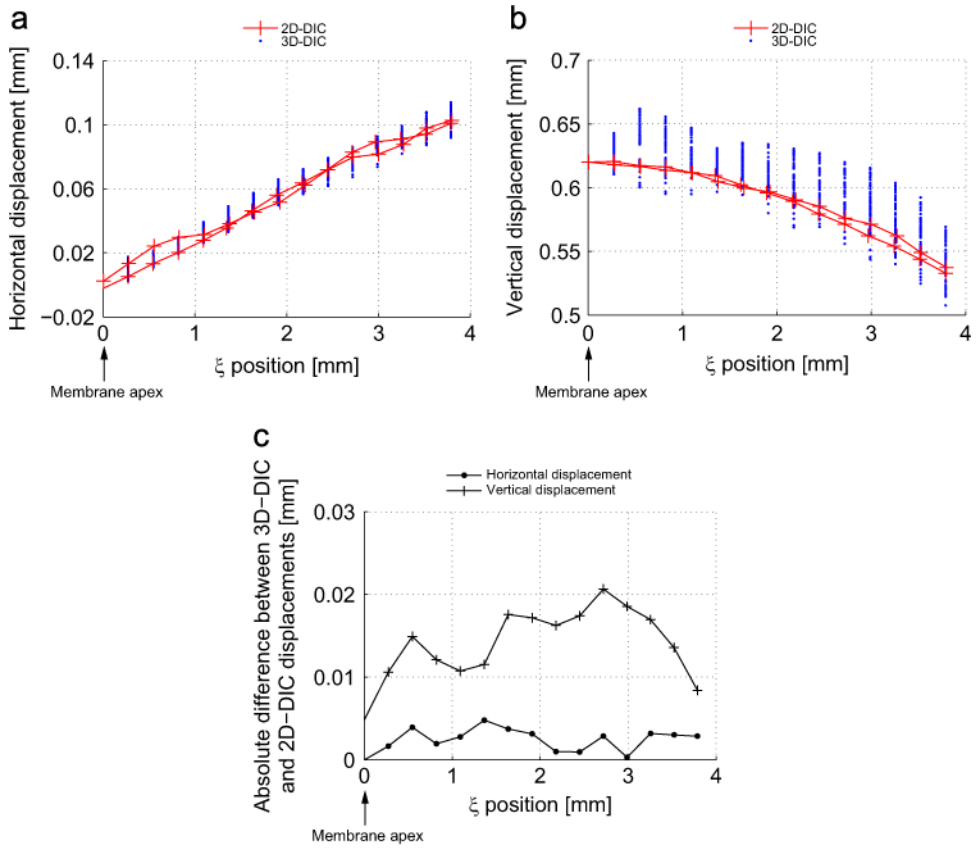

Fig. 5.

(a) Horizontal displacement and (b) vertical displacement for the 2D meridians and the 3D meridians from quadrants 1 and 3. (c) Absolute difference between the 3D-DIC and 2D-DIC displacement components, averaged over the 2 meridians or 60 meridians considered, at each ξ position.

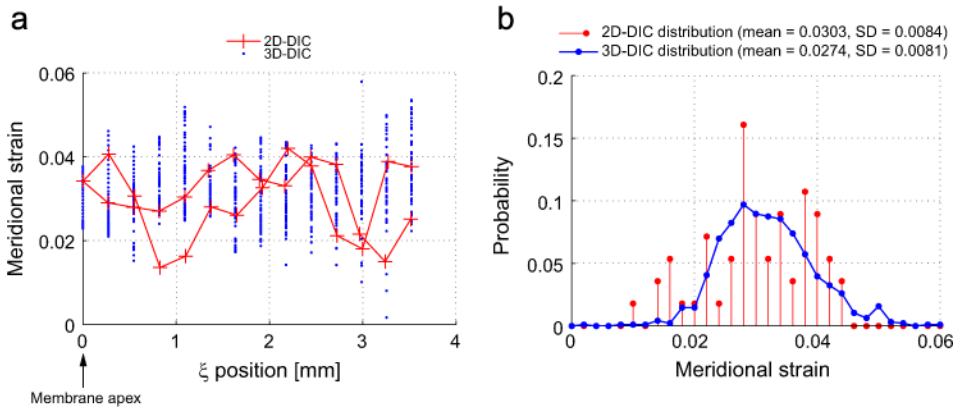

Fig. 6.

(a) Meridional strain for the 2D meridians and the 3D meridians from quadrants 1 and 3. (b) Probability distributions for the 2D-DIC and 3D-DIC meridional strain, calculated using a 0.0020 strain bin size.